Nonlinear interaction of vector solitons inside birefringent optical fibers

Prannay Balla and Govind P. Agrawal

Nonlinear interaction of vector solitons inside birefringent optical fibers

Prannay Balla and Govind P. Agrawal

The Institute of Optics, University of Rochester, Rochester, NY 14627, USA

(Dated: June 22, 2018)

The nonlinear interaction of two temporally separated solitons inside optical fibers has been studied in the scalar case in which both solitons remain linearly polarized during their mutual interaction. Here we consider two arbitrarily polarized vector solitons inside birefringent optical fibers where they interact nonlinearly. We develop a general formalism based on two coupled nonlinear Schrödinger equations that include both the Raman and the Kerr nonlinearities. We use it to study how the two vector solitons evolve in the temporal, spectral, and polarization domains in optical fibers exhibiting no, medium, or large birefringence. The attractive force that leads to collisions of two in-phase solitons in isotropic fibers is affected considerably by fiber's birefringence. In particular, no collisions occur even in the case of medium birefringence. Rather, the two vector solitons exchange energy as they approach each other and then move away from each other. Moreover, considerably energy is shed in the form of dispersive waves. Polarization of the two solitons is found to be affected considerably by the fiber nonlinearity in the case of medium birefringence but linear effects dominate its evolution in fibers with large birefringence.

I. INTRODUCTION

The nonlinear interaction of two neighboring solitons inside optical fibers has been studied extensively since the 1980s [1–5]. Depending on their relative amplitudes and phases, the two solitons may attract or repel each other. More recently, the effects of Raman scattering on two interacting optical solitons have been studied [6–9]. In all of these studies, optical pulses were assumed to remain linearly polarized during their propagation inside the optical fiber, and a scalar nonlinear Schrödinger (NLS) equation was used to describe the nonlinear interaction between two temporally separated solitons.

The vectorial nature of an electromagnetic field cannot be ignored in birefringent optical fibers that are known to support vector solitons and whose description requires two coupled NLS equations [5]. Here we use the term "vector soliton" in its broad sense, recalling that such solitons are in fact solitary waves that propagate undistorted over long fiber lengths but are not guaranteed to survive mutual collisions. A vector soliton consists of two orthogonally polarized components that move at the same speed by shifting their spectra to compensate for polarization-mode dispersion of the fiber. This is often referred to as soliton trapping, occurring when the nonlinear phenomenon of cross-phase modulation (XPM) produces spectral shifts in the opposite directions such that both components move together in the time domain [10–13].

The coupled NLS equations have been used extensively in several different contexts [5]. Many studies focus on a single vector soliton [14–21], while others consider the interaction of two orthogonally polarized but temporally separated pulses along the slow and fast axes of a birefringent fiber [22–27]. The more general case involving the interaction of two arbitrary polarized, vector solitons has attracted relatively little attention [28, 29]. Vector solitons have also been studied in the context of fiber lasers where fiber's birefringence cannot always be ignored [30–33]. The interaction between two such vector solitons can lead to the formation of specific bound states called soliton molecules [34–37].

In this paper, we focus on the case of two temporally separated vector solitons, realized by launching two closely spaced, identically polarized, optical pulses of the same wavelength inside a birefringent optical fiber, where they interact nonlinearly through the Kerr and the Raman effects. We discuss in section 2 the underlying physical model and describe the numerical method employed. In section 3 we consider briefly the case of isotropic fibers. In section 4 we consider fibers with medium birefringence with and without the Raman contribution. Numerical simulations are used to see how the interaction between two vector solitons is affected by fiber's birefringence and its nonlinearity. Fibers with large birefringence are discussed in section 5. The impact of relative phase of two solitons on the nonlinear interaction is studied in section 6 and main conclusions are summarized in section 7.

II. NUMERICAL MODEL

We consider a single-mode fiber with an elliptical or stressed core such that it supports two orthogonally polarized modes with the same spatial profile but different propagation constants denoted by $\beta_x(\omega)$ and $\beta_y(\omega)$. Two closely spaced, identically polarized, optical pulses of the same wavelength are launched into this fiber. Their evolution can be studied by expanding $\beta_j(\omega)$ with $j = x, y$ in a Taylor series around the pulse's central frequency ω_0 as

$$\beta_j(\omega) = \beta_{0j} + \beta_{1j}(\omega - \omega_0)$$
$$+ \frac{1}{2}\beta_{2j}(\omega - \omega_0)^2 + \frac{1}{6}\beta_{3j}(\omega - \omega_0)^3 + \dots \quad (1)$$

Following a standard procedure [5], we write the total electric field as

$$\mathbf{E}(\mathbf{r}, t) = \text{Re}\left[\hat{\mathbf{x}}A_x e^{i(\beta_{0x} - i\omega_0 t)} + \hat{\mathbf{y}}A_y e^{i(\beta_{0y} - i\omega_0 t)}\right] \quad (2)$$

and obtain the following two coupled NLS equations for the slowly varying amplitudes $A_j(z, t)$:

$$\frac{\partial A_j}{\partial z} + \beta_{1j}\frac{\partial A_j}{\partial t} + \frac{i\beta_2}{2}\frac{\partial^2 A_j}{\partial t^2} - \frac{\beta_3}{6}\frac{\partial^3 A_j}{\partial t^3} = Q_j, \quad (3)$$

where $j = x, y$ and we retained the dispersive terms up to third order and assumed that β_2 and β_3 are the same for the two polarization components. Different values of β_{1x} and β_{1y} lead to different group velocities for the two polarization components, resulting in a differential group delay (DGD).

Before writing the nonlinear terms Q_x and Q_y, we convert Eq. (3) into a dimensionless form by using the soliton units [5]:

$$\tau = (t - \bar{\beta}_1 z)/T_0, \qquad \xi = z/L_D,$$
$$A_x = u\sqrt{P_0}e^{-i\Delta\beta z/2}, \quad A_y = v\sqrt{P_0}e^{i\Delta\beta z/2}, \quad (4)$$

where T_0 and P_0 are related to the width and the peak power of input pulses, $L_D = T_0^2/|\beta_2|$ is the dispersion length of the fiber, and

$$\bar{\beta}_1 = (\beta_{1x} + \beta_{1y})/2, \qquad \Delta\beta = \beta_{0x} - \beta_{0y}, \quad (5)$$

with $\Delta\beta$ representing fiber's birefringence. The resulting coupled NLS equations take the final form

$$i\left(\frac{\partial u}{\partial \xi} + \delta\frac{\partial u}{\partial \tau}\right) + bu + \frac{1}{2}\frac{\partial^2 u}{\partial \tau^2} + i\delta_3\frac{\partial^3 u}{\partial \tau^3} = Q_x L_D, \quad (6)$$

$$i\left(\frac{\partial v}{\partial \xi} - \delta\frac{\partial v}{\partial \tau}\right) - bv + \frac{1}{2}\frac{\partial^2 v}{\partial \tau^2} + +i\delta_3\frac{\partial^3 v}{\partial \tau^3} = Q_y L_D, \quad (7)$$

where we assumed $\beta_2 < 0$ and introduced three parameters

$$b = \frac{T_0^2(\Delta\beta)}{2|\beta_2|}, \quad \delta = \frac{T_0}{2|\beta_2|}(\beta_{1x} - \beta_{1y}), \quad \delta_3 = \frac{\beta_3}{3|\beta_2|T_0}. \quad (8)$$

Physically, b is related to fiber's birefringence, δ to its DGD, and δ_3 to its third-order dispersion (TOD).

The nonlinear terms on the right side of Eqs. (6) and (7) include both the Kerr and Raman nonlinearities [5] and are given by

$$Q_x = \frac{iN^2}{L_D}\left(1 + \frac{i}{\omega_0}\frac{\partial}{\partial t}\right)\left[(1 - f_R)\left(|u|^2 u + \frac{2}{3}|v|^2 u + \frac{1}{3}v^2 u^*\right)\right.$$
$$\left. + f_R\left(u[h_1 \otimes |u|^2 + h_2 \otimes |v|^2] + v[h_3 \otimes (uv^* + vu^*)]\right)\right], \quad (9)$$

$$Q_y = \frac{iN^2}{L_D}\left(1 + \frac{i}{\omega_0}\frac{\partial}{\partial t}\right)\left[(1 - f_R)\left(|v|^2 v + \frac{2}{3}|u|^2 v + \frac{1}{3}u^2 v^*\right)\right.$$
$$\left. + f_R\left(v[h_1 \otimes |v|^2 + h_2 \otimes |v|^2] + v[h_3 \otimes (uv^* + vu^*)]\right)\right], \quad (10)$$

where a $\otimes$ represents convolution, $N = (\gamma P_0 L_D)^{1/2}$ is the soliton number, and f_R represents the fractional contribution of the delayed Raman response governed by the time-dependent functions $h_1(t)$, $h_2(t)$, and $h_3(t)$. These functions are related to the isotropic and anisotropic parts of the nuclear response, $h_a(t)$ and $h_b(t)$ as [38, 39]

$$h_1(t) = (f_a + f_c)h_a(t) + f_b h_b(t), \quad h_2(t) = f_a h_a(t), \quad (11)$$

$$h_3(t) = [f_c h_a(t) + f_b h_b(t)]/2, \quad (12)$$

where $f_a = 0.75$, $f_b = 0.21$, and $f_c = 0.04$. The explicit form of the Raman response functions for silica fibers is [40]

$$h_a(t) = \frac{\tau_1^2 + \tau_2^2}{\tau_1\tau_2^2}\exp\left(-\frac{t}{\tau_2}\right)\sin\left(\frac{t}{\tau_1}\right), \quad (13)$$

$$h_b(t) = [(2\tau_b - t)/\tau_b^2]\exp(-t/\tau_b), \quad (14)$$

with $\tau_1 = 12.2$ fs, $\tau_2 = 32$ fs, $\tau_b = 96$ fs, and $f_R = 0.245$ for silica fibers.

We solve the coupled NLS equations (6) and (7) numerically with an input field in the form

$$u(0, \tau) = \cos\theta[\text{sech}(\tau + q_0) + e^{i\phi}\text{sech}(\tau - q_0)], \quad (15)$$

$$v(0, \tau) = \sin\theta e^{i\psi}[\text{sech}(\tau + q_0) + e^{i\phi}\text{sech}(\tau - q_0)], \quad (16)$$

where θ and ψ are the angles used to indicate the polarization of two input pulses separated by $T_s = 2q_0 T_0$ initially. We choose $T_0 = 100$ fs (full width at half maximum about 180 fs). This input corresponds to two arbitrarily polarized pulses that are separated in time but have the same temporal shape and optical spectra. We assume that both pulses are linearly polarized ($\psi = 0$) and choose $\theta = 45°$ for which the x and y components have the same amplitude. Any arbitrary state of polarization (SOP) on the Poincaré sphere can be chosen by varying these two angles. We choose $q_0 = 3.5$ in our numerical simulations to ensure that tails of two pulses overlap to some extent for them to interact nonlinearly. The relative phase ϕ between two pulses is set to zero to focus on the in-phase case that leads to an initial attraction between two vector solitons. Other values of ϕ are considered in Section 6.

For the numerical simulations, we use a method known as RK4IP, standing for the fourth-order Runge–Kutta method in the interaction picture [41]. The basic idea is to first write Eqs. (6) and (7) in the form

$$\frac{\partial u}{\partial \xi} = D_1 u + N_1, \quad \frac{\partial v}{\partial \xi} = D_2 u + N_2, \quad (17)$$

where D_j is a linear differential operator and $N_j(u, v)$ is a nonlinear function with $j = 1, 2$. By taking the Fourier transform with respect to τ, these can be written as

$$\frac{\partial \tilde{u}}{\partial \xi} = D_1(\omega)\tilde{u} + \tilde{N}_1, \quad \frac{\partial \tilde{v}}{\partial \xi} = D_2(\omega)\tilde{v} + \tilde{N}_2, \quad (18)$$

where a tilde denotes the Fourier-transform operation. As D_j becomes a known function $D_j(\omega)$ in the frequency domain, we can eliminate it by writing Eq. (18) in the interaction picture used often in quantum mechanics:

$$\frac{\partial \tilde{u}'}{\partial \xi} = \tilde{N}_1 e^{-D_1 \xi}, \quad \frac{\partial \tilde{v}'}{\partial \xi} = \tilde{N}_2 e^{-D_2 \xi}, \qquad (19)$$

where u' and v' in the interaction picture are related to u and v as $u = u'e^{D_1\xi}$ and $v = v'e^{D_2\xi}$. This set of ordinary differential equations is solved in the RK4IP method on a frequency grid chosen to cover the entire spectral bandwidth of solitons. The nonlinear terms N_j are first calculated in the time domain and then converted to the frequency domain using the fast-Fourier-transform (FFT) algorithm.

Most Numerical simulations were performed with a temporal window in the range $-200 < \tau < 200$ with $N = 2^{14}$ FFT points. A wider window ($-1000 < \tau < 1000$) was needed in the high-birefringence case. In all cases, temporal window was wide enough that no radiation reached the boundaries of the computational window over the simulated fiber length. The choice of N was dictated by the requirement that the corresponding frequency window is wide enough and has sufficient resolution to provide accurate results. We choose the peak power of input pulses such that $N = 1$ so that both pulses correspond to fundamental solitons. The birefringence parameters b and δ are fiber specific and can vary over a wide range. We decided to focus on two fibers with medium and large birefringence. In the former case, we take $b = 0.1$ and $\delta = 0.1$ but increase these values to $b = 10$ and $\delta = 1$ in the high-birefringence case. It is often argued that b can be set to zero in the case of high birefringence because of an averaging effect produced by rapid changes in the relative phase of the two polarization components [5]. We decided not to do so to reveal the residual effects when b is not too large. The only other parameter we need to specify is δ_3. We choose $\delta_3 = 0.1$ as a representative value for silica fibers.

To characterize the SOP evolution, it is common to trace the trajectory of the Stokes vector on the Poincaré sphere. However, in our case the SOP can be nonuniform in time at a given distance while also varying along the fiber length. To isolate length variations, SOP evolution is shown at the the intensity peak of the two vector solitons. The magnitude S_0 and components of the Stokes vector are calculated from A_x and A_y using

$$S_0 = |A_x|^2 + |A_y|^2, \quad S_1 = |A_x|^2 - |A_y|^2, \qquad (20)$$
$$S_2 = 2\mathrm{Re}(A_x A_y^*), \quad S_3 = -2\mathrm{Im}(A_x A_y^*). \qquad (21)$$

We map the sphere onto a two-dimensional plane using the Hammer projection. We use this projection to visualize the entire Poincaré sphere in a single plot, avoiding two separate plots displaying the front and the back of this sphere. The longitude λ and the latitude χ are calculated first using $\tan(2\lambda) = S_2/S_1$ and $\sin(2\chi) = S_3/S_0$.
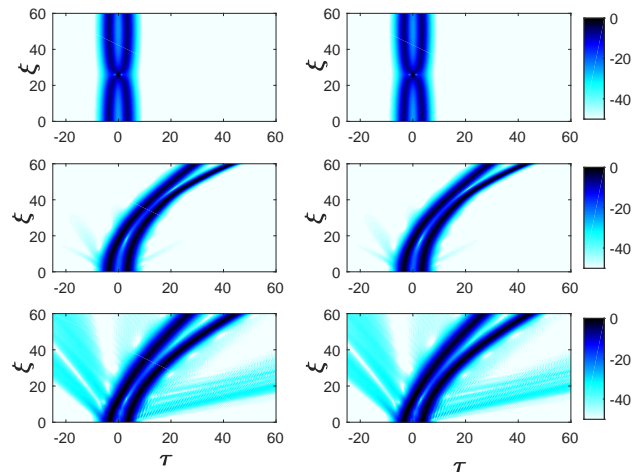

FIG. 1. Evolution of two temporally separated vector solitons in isotropic fibers with the Kerr nonlinearity alone (top row) and with Raman nonlinearity included (middle row). The TOD is also included in the bottom row. Temporal profiles of the x (left) and y (right) components are shown with the intensity on a decibel scale using dimensionless variables.

These are used to calculate the coordinates for the Hammer projection as [42]

$$x_h = \frac{2\sqrt{2}\cos(2\chi)\sin(\lambda)}{\sqrt{1 + \cos(2\chi)\cos(\lambda)}}, \quad y_h = \frac{\sqrt{2}\sin(2\chi)}{\sqrt{1 + \cos(2\chi)\cos(\lambda)}}. \qquad (22)$$

III. FIBERS WITH NO BIREFRINGENCE

Before considering the general case of birefringent fibers, it is useful to consider the ideal case of isotropic fibers for which $b = 0$ and $\delta = 0$. The TOD effects are also ignored initially by setting $\delta_3 = 0$ so that solitons can evolve in an ideal fashion without any perturbation. This case serves as a reference and can be used to isolate the effects of birefringence and TOD studied in later sections.

The top row in Figure 1 shows the temporal evolution of two vector solitons over 60 dispersion lengths ($\xi = 0$–60) as a function τ and ξ. The Raman effects have been turned off by setting $f_R = 0$ so that the interaction of two vector solitons is governed by only the fast-responding Kerr nonlinearity. The main feature is that the two vector solitons attract each other and collide at a distance of about $\xi = 25$, after which they separate and recover their original spacing around $\xi = 50$. This process repeats periodically just as it does for two scalar in-phase solitons [5]. The spectra (not shown) of two vector solitons also exhibit an oscillatory evolution and become considerably broader when two solitons overlap and become narrower during each collision. It is remarkable that both vector solitons survive multiple collisions in spite of the fact that the underlying propagations equations are not

integrable (in the sense of inverse scattering theory).

Inclusion of the the Raman nonlinearity (middle row) changes this interaction scenario drastically. First, each pulse slows down because of the Raman-induced red shift of its spectrum [5]. This red shift is related to intra-pulse Raman scattering and is also called the soliton self-frequency shift (SSFS). It bends the soliton trajectory toward the right in Fig. 1. The Kerr nonlinearity still provides an attractive force that brings the two solitons closer initially. However, two pulses never collide and begin to separate from each other at a distance of about $40L_D$. Moreover, energy transfer (of about 18%) takes place form the leading pulse (on left) to the trailing pulse (on right). Since a soliton must conserve $N = 1$ and since N is related to pulse energy $E_p = 2P_0T_0$ as

$$N^2 = \gamma P_0 L_D = \gamma P_0 T_0^2/|\beta_2| = \gamma E_p T_0/(2|\beta_2|), \quad (23)$$

it follows that a soliton gaining energy must become narrower as the one losing energy broadens. The same behavior also occurs for scalar solitons and is a consequence of the delayed nature of the Raman nonlinearity [9]. As discussed later, energy transfer depends on the relative phase ϕ in Eq. (15) of the two solitons.

The bottom row of Fig. 1 shows what happens when the TOD is included using $\delta_3 = 0.1$. As is well known, TOD perturbs each soliton and forces it to shed some energy in the form of a dispersive wave [5]. Rapid spreading of such dispersive waves is evident in Fig. 1. The spectra (not shown) also develop a new spectral peak located at a specific frequency that satisfied the corresponding phase-matching condition. The amount of energy lost through dispersive waves is relatively small ($< 2\%$). However, our results reveal that the presence of TOD also reduces the extent of energy transfer between two vector solitons (from 18% to 11%). This can be deduced from the bottom row of Fig. 1 by noting that the right soliton is not as narrow as in the middle row. We include TOD using $\delta_3 = 0.1$ in the following discussion.

IV. FIBERS WITH MEDIUM BIREFRINGENCE

In this section we focus on an optical fiber with medium birefringence and choose $b = 0.1$ and $\delta = 0.1$. To gain physical insight that helps us in interpreting the effects of Raman nonlinearity, we first ignore it by setting $f_R = 0$. The impact of Raman nonlinearity on the interaction of two scalar solitons inside isotropic fibers has been studied in Ref. [9]. The results here extend this study to the case of vector solitons forming in birefringent fibers.

A. Kerr nonlinearity alone

The question we ask is how fiber's birefringence affects the interaction of two vector solitons. Figure 2 answers this question in the case of medium birefringence
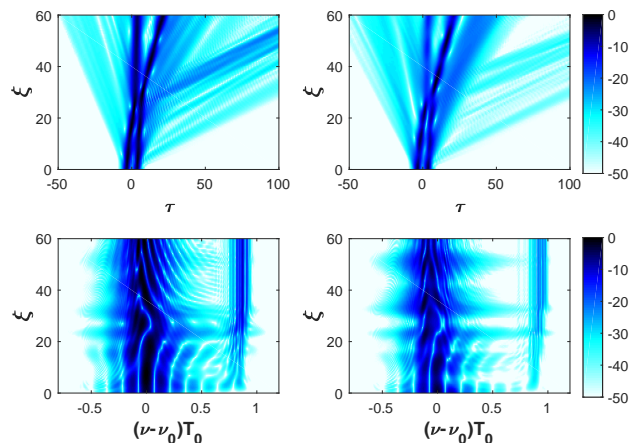

FIG. 2. Temporal (top) and spectral (bottom) evolutions over $60L_D$ for the x (left) and y (right) polarized components of the two interacting vector solitons inside a medium-birefringence fiber with only Kerr nonlinearity. The intensity is coded on a decibel scale using dimensionless variables.

($\delta = 0.1$, $b = 0.1$). The temporal (top row) and spectral (bottom row) intensity profiles are displayed in this figure over $60L_D$ for the x (left column) and y polarized components of the two interacting vector solitons considering only the Kerr nonlinearity. The top row of Fig. 2 should be compared to the top row of Fig. 1 showing the case of a fiber without any birefringence. The main feature is the absence of any mutual collision. The two solitons do move closer but they never collide. As expected, the two components of each vector soliton move at the same speed, in spite of a group-velocity mismatch resulting from the DGD (included through the parameter δ). This is a consequence of the cross-phase modulation that shifts the pulse spectra in the opposite directions such that the two components trap each other and move at a common speed [11].

Tilting of the soliton trajectory toward the right in Fig. 2 is due to the effects of TOD included through $\delta_3 = 0.1$. We have verified that a left tilt occurs for $\delta_3 = -0.1$, and no tilt occurs for $\delta_3 = 0$. Solitons also shed some energy in the form of dispersive waves. The spectral peak in the pulse spectra near $(\nu - \nu_0)T_0 = 0.8$ (bottom row) indicates that, although some energy is shed within the first few dispersion lengths, much more energy is fed to this dispersive wave at a distance of about $25L_D$. Recall from Fig. 1 that this is the distance at which two solitons collide in the absence of birefringence. A collision does not occur in the presence of birefringence, but pulses come closer, become narrower, and their spectra broaden at this distance. Also the left soliton transfers energy to the right soliton. We estimated numerically that the left soliton losses 38% of its energy at a distance of $90L_D$, while the right soliton gains only 14%. The difference of 24% is shed to dispersive waves. The temporal and spectral oscillations with ξ seen in Fig. 2 are related to changes in the SOP of the two interacting
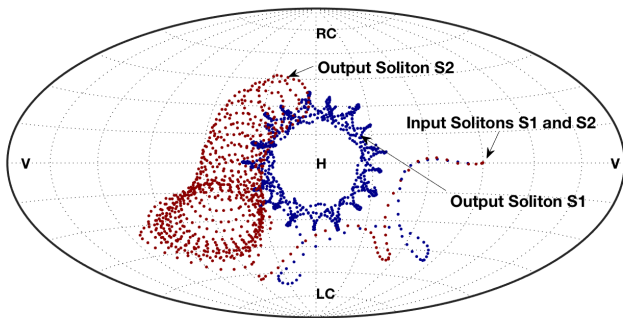
FIG. 3. Evolution of SOP for the leading (S1, blue, near center) and trailing (S2, gray or red) solitons over $400L_D$ inside a fiber with medium birefringence. In this Hammer projection of the Poincaré sphere, the dashed longitude and latitude lines are $15°$ apart, with H and V marking horizontal and vertical linear SOPs. The poles represent right-circular (RC) and left-circular (LC) SOPs.

FIG. 4. Temporal (top) and spectral (bottom) evolutions over $80L_D$ for the x (left) and y (right) polarized components of the two interacting vector solitons inside a fiber with medium birefringence. All parameters are the same as in Fig. 2 except that the Raman contribution has been turned on.

vector solitons that we discuss next.

Figure 3 shows the evolution of the SOP of the leading soliton S1 (blue curve) and the trailing soliton S2 (red curve) along the length of a fiber with medium birefringence. The input SOP of both solitons is linearly polarized at $45°$ from the x axis (marked by an arrow). The SOP changes initially in an identical fashion for both solitons but, after a few dispersion lengths, the SOPs of two solitons follow different trajectories on the Poincaré sphere. It turns out that the SOP evolution can be understood qualitatively using the theory developed for continuous-wave (CW) beams. In this theory the Stokes vector evolves as [5]

$$dS/dz = W \times S, \qquad W = \Delta\beta\hat{x} - 2\gamma(S_3/3)\hat{z}. \quad (24)$$

Physically speaking, the Stokes vector rotates on the Poincaré sphere around an axis oriented along the vector W that has a linear part and a nonlinear part. The linear birefringence forces S to rotate around the x axis, while the nonlinear birefringence forces it to rotate around the z axis. In the case of medium birefringence, the two rotations compete, leading to the patterns seen in Fig. 3. Since $S_3 = 0$ initially, the linear birefringence dominates first and makes the SOP of each soliton slightly elliptical. A finite value of the resulting S_3 then induces nonlinear polarization rotation around the z axis. Since S_3 becomes larger farther away the SOP is from the equator, the nonlinear term dominates as the soliton's SOP moves toward the poles. The reason that two trajectories are so different is related to the Kerr-induced energy transfer from S1 to S2. Since no transfer occurs in the absence of birefringence, it is a new birefringence effect. It can be understood by noting that the Kerr nonlinearity can lead to energy transfer when the two solitons have different phases [9]. Since a relative phase difference is always induced by the birefringence, its presence leads to energy transfer. Notice that energy transfer breaks the symmetry between two solitons and makes the sit-
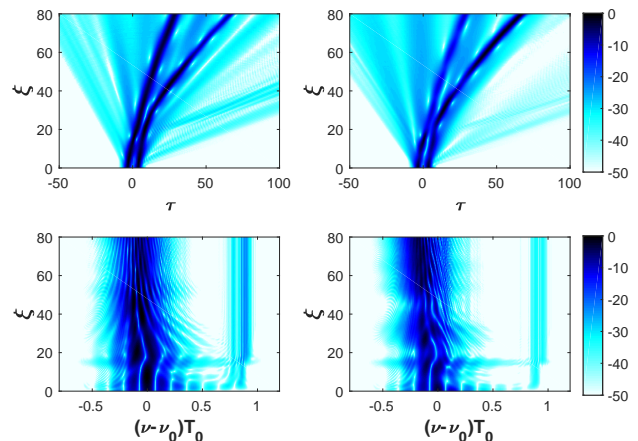
uation asymmetric with respect to the two polarization components.

B. Raman nonlinearity included

Figure 4 shows how the interaction behavior shown in Fig. 2 is modified when the Raman contribution to the fiber nonlinearity is included. Both the temporal and spectral intensity profiles of the two polarization components look similar qualitatively but have substantial quantitative differences. For example, the vector nature of each soliton is maintained even when the Raman contribution is included in the sense that the two polarization components move at the same speed, in spite of the birefringence-induced DGD, through XPM-induced spectral shifts in the opposite directions. In addition, both spectra shift toward the red because of SSFS. As a result, although temporal trajectories tilt toward the right for both solitons, this tilt is larger for the trailing soliton because the XPM and Raman shifts are in the same direction for this soliton. For this reason, the spectra are not identical for the two polarization components.

Another noticeable effect of the delayed Raman nonlinearity is a reduction in the energy lost to dispersive waves. Even though dispersive radiation is clearly evident in both Figs. 2 and 4, its energy content is much smaller in the Raman case (down to about 10% from 24%). This is evident from the spectral peak located near $(\nu - \nu_0)T_0 = 0.8$ whose strength is much reduced in Fig. 4. It can also be seen in the temporal evolution in Fig. 2, where a relatively large amount of energy is lost to dispersive waves near $\xi = 25$; the corresponding radiation is absent in Fig. 4. We estimated numerically the energy loss for the leading soliton at a distance of $90L_D$ to be 23% and 38%, with and without the Raman
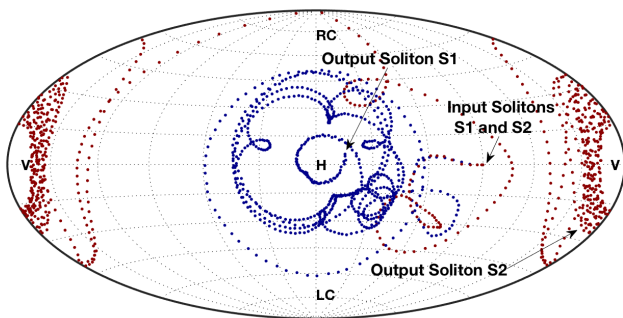
FIG. 5. Same as Fig. 3, except that the Raman contribution has been turned on.

FIG. 6. Temporal (top) and spectral (bottom) evolutions over $200L_D$ of the x (left) and y (right) polarized components of the two interacting vector solitons inside a fiber with large birefringence with only Kerr nonlinearity.

FIG. 7. Same as Fig. 3 except that fiber has a relatively large birefringence. Black dots correspond to a third soliton discussed in the text

contribution respectively.

One should ask how the Raman contribution affects the SOP of two vector solitons. Figure 5 shows SOP evolution along the fiber when both the Kerr and Raman contributions are included. It should be compared with Fig. 3 where the Raman contribution was ignored. It is evident that the SOPs of the two solitons evolve quite differently when the Raman effects are included. The initial evolution is similar to that in Fig. 3 in the sense that the SOPs of two solitons remain identical while becoming elliptical and moving toward the center. However, after a few dispersion lengths, the SSFS changes the SOP in such a fashion that trajectory S1 of the leading soliton moves toward the center (near H), while that of the trailing soliton S2 moves away from center (near V), in sharp contrast with the case of purely Kerr nonlinearity. The SOPs of both solitons still rotates in a circular fashion, as dictated by the linear birefringence that is not affected by the Raman effects. We note that one cannot use CW theory to understand these SOP changes because SSFS occurs only for short optical pulses.

V. FIBERS WITH LARGE BIREFRINGENCE

In this section we consider the case of fibers with a relatively large birefringence by choosing $b = 10$ and $\delta = 1$. As we did for medium-birefringence case, we first ignore the Raman effect by setting $f_R = 0$ before including it. The impact of Raman nonlinearity on the interaction of two scalar solitons in isotropic fibers has been considered before [9]. The results here extend this study to the case of vector solitons.

A. Kerr nonlinearity alone

Figure 6 shows the temporal and spectral evolutions of the two polarization components over $200L_D$ for a fiber with high birefringence. It should be compared to Fig. 2 where the case of medium birefringence is shown for the same parameter values. The differences in the two cases are quite remarkable and stem mostly from
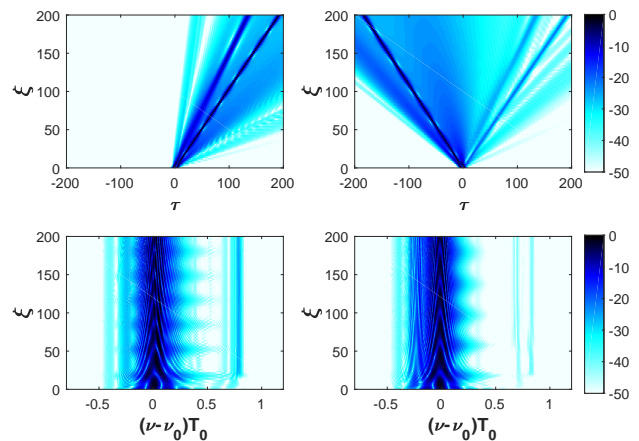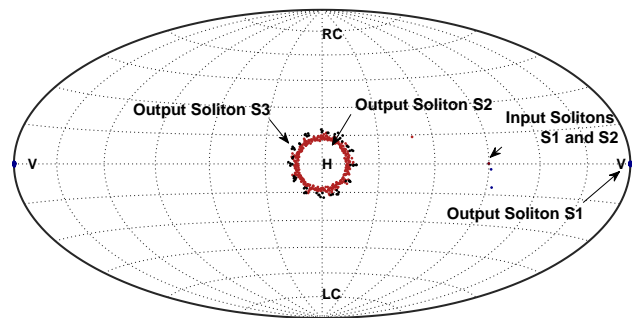
a larger DGD between the x and y polarization components. More specifically, a relatively large difference in the group velocities of the two components (resulting from $\delta = 1$) destroys their mutual trapping. The x component of each pulse captures a small fraction of energy of the y component and forms a vector soliton (two dark lines tilted to the right in Fig. 6). The remaining energy of the y component remains polarized along the y axis and forms a scalar soliton that moves faster than the two vector solitons (single dark line tilted to the left in Fig. 6). All solitons emit their own dispersive waves, resulting in multiple spectral lines near $(\nu - \nu_0)T_0 = 0.8$ in the bottom row.

The SOP evolution in fibers with large birefringence is shown in Fig. 7, and it should be compared to the medium-birefringence case shown in Fig. 3. Clearly, dramatic changes are induced in the SOP of each soliton by larger values of the parameters b and δ. The initial SOP of the two solitons (marked by an arrow) changes quickly but in very different ways. The SOP of the vector soliton S2 moves toward the center and rotates in a circular fashion around it (red trace). The second vector

soliton has a SOP (black dots) that nearly matches that of S2. In contrast, the SOP of the scalar soliton S1 jumps toward the edges. Since S1 has no x-polarized partner, it must remain polarized along the y axis. This is why the SOP of the scalar soliton does not change and lies at the location marked V in Fig. 7. These features can be understood qualitatively from Eq. (21). In the case of high birefringence, the linear part of the vector $\mathbf{W}$ dominates compared to the nonlinear part and forces the SOP to rotate around the x axis (normal to the plane of the figure). This is the reason why the two vector solitons follow a circular path around the center in Fig. 7.

B. Raman nonlinearity included

Finally, we consider the impact of Raman nonlinearity in fibers exhibiting high birefringence. Figure 8 shows the temporal and spectral evolutions of the two polarization components over $200L_D$ in this case. It should be compared with Fig. 6, where the case of high birefringence is shown without the Raman contribution. In both cases, a relatively large difference in the group velocities of the two components destroys their mutual trapping. Once again two pulses forms two vector solitons but only a small fraction of the y-component energy is captured. the remaining energy in the y component propagates as a scalar soliton moving faster than the vector solitons. The Raman nonlinearity plays a minor role and does not introduce new qualitative features. It red-shifts the spectrum of each soliton through SSFS and slows it down. As a result, the tilt of the soliton trajectories are different ansd spectra are slightly shifted toward the red side in Fig. 8 compare to Fig. 6. Otherwise, the Raman-induced SSFS has a relatively minor effect on the overall evolution process.

The SOP of the two solitons whose evolution is shown in Fig. 8 was also simulated numerically. However, the resulting plot is virtually identical to that shown in Fig. 7. Although high birefringence affects the SOP evolution drastically, the inclusion of Raman contribution does not introduce any further changes. The reason is that the SOP evolution is totally dominated by the large linear birefringence of the fiber (or by the relatively large vales of the parameters b and δ). The initial SOP of the vector soliton S2 changes very quickly (blue curve) and rotates in a circular fashion around the center, as dictated by this linear birefringence. The SOP of the scalar soliton does not change at all because it contains only the y-polarized light. We conclude that intrapulse Raman scattering does not have a significant impact on the soliton dynamics in the case of high birefringence. It causes a red shift in the spectra of both solitons, but the impact of that red shift on the SOPs of the two solitons is relatively minor.
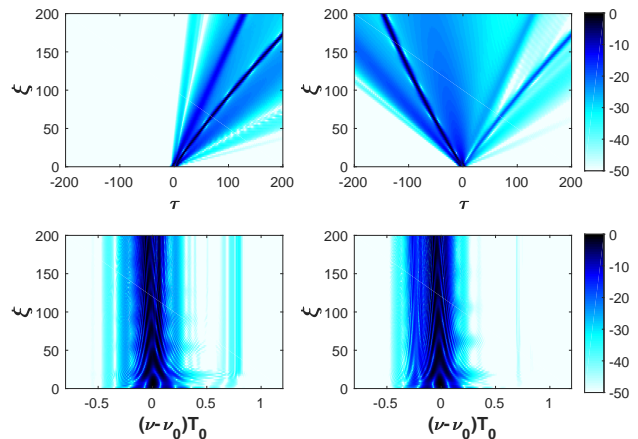

FIG. 8. Temporal (top row) and spectral (bottom row) evolutions over $50L_D$ of the x (left) and y polarized components of the two interacting vector solitons inside an high birefringence fiber. All parameters are the same as in Fig. 6 except that the Raman contribution has been turned on.

VI. IMPACT OF THE RELATIVE PHASE

It is well known that the relative phase ϕ of two solitons affects drastically their interaction inside isotropic fibers [1]. The attractive force that leads to collision in Fig. 1 for $\phi = 0$ becomes a repulsive force even for $\phi = 45°$. Also, even though no energy exchange occurs when $\phi = 0$, some energy is exchanged between two solitons even for relatively small values of ϕ. Moreover, inclusion of the Raman nonlinearity leads to energy transfer even for two in-phase solitons [9]. As discussed in Section 3, such an exchange also occurs for two in-phase vector solitons.

In this section we consider the dependence of energy transfer on the relative initial phase of two vector solitons. More specifically, we focus on the case of Section 4 where two in-phase vector solitons were considered inside a medium-birefringence fiber. For simplicity, we neglect the Raman contribution to the fiber nonlinearity and vary the relative phase ϕ of two input pulses. For each value of ϕ we solve Eqs. (6) and (7) over a distance exceeding $\xi = 100$ to enure that a kind of steady state has reached. We calculate the energy loss or gain of each soliton at that distance relative to its input energy. Figure 9 shows this loss/gain as a function of ϕ.

Several points are noteworthy. First the energy is always transferred from the leading soliton S1 to the trailing soliton S2. Second, not all energy lost from S1 goes to S2 because both solitons also shed energy in the form of dispersive waves. The DW curve in Fig. 2 shows the fraction of total energy lost to dispersive waves. Third, energy transfer is relatively large for values of the relative phase between 0 and $\pi/4$, with a maximum occurring near $\phi = 30°$ where the S1 soliton loses almost 70% of its energy. Fourth, the energy lost to dispersive waves is relatively large (about 25%). As mentioned earlier, most
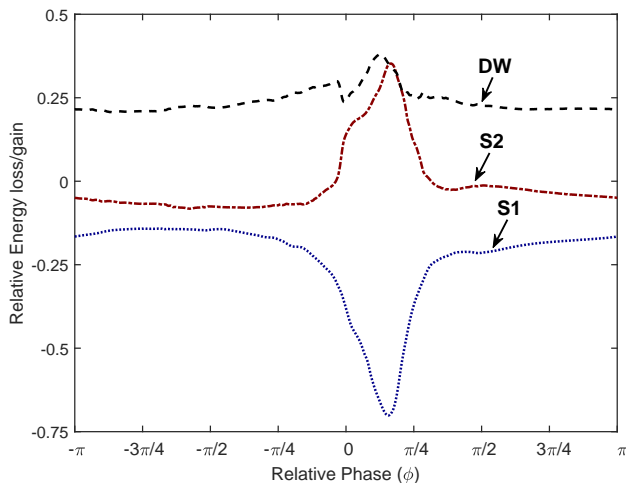
FIG. 9. Relative energy loss or gain of each soliton at a distance of $110L_D$ for a fiber with medium birefringence. All other parameters are the same as in Fig. 2. The DW curve shows the energy shed in the form of dispersive waves.

of this loss can be attributed to fiber's birefringence. If we set birefringence to zero, only the TOD transfers energy to a dispersive wave whose energy level is reduced to below 2%.

As a specific example, consider the case of two in-phase solitons. The S1 soliton loses 38% of its energy of which 14% is transferred to the S2 soliton. When we also include the Raman nonlinearity, S1 soliton loses 23% of its energy but only 12% of it goes to the trailing soliton, remaining 11% is lost to dispersive waves. It appears from these lower numbers that the Raman nonlinearity actually helps in stabilizing the two vector solitons. However, this advantage disappears for fibers with a large birefringence. Our numerical results show that both solitons lose a large fraction of their energy (38%) to dispersive waves in a fiber with large birefringence. We conclude that large values of birefringence perturbs vector solitons drastically and eventually lead to their destruction.

VII. CONCLUDING REMARKS

In this paper we have considered the nonlinear interaction of two arbitrarily polarized vector solitons inside birefringent optical fibers. We develop a general formalism based on two coupled NLS equations that include both the Raman and the Kerr nonlinearities. We use them to study how the two vector solitons evolve in the temporal, spectral, and polarization domains in optical fibers exhibiting no, medium, or large birefringence. The main results can be summarized as follows.

The attractive force that leads to collisions of two in-phase solitons in isotropic fibers is affected considerably by fiber's birefringence. In particular, no collisions occur even in the case of medium birefringence. Rather, the two vector solitons exchange energy as they approach each other and then move away from each other. If the Raman nonlinearity is included, energy is always transferred from the leading soliton to the trailing soliton [9]. The fraction of energy transfer depends on the relative phase of the two solitons and on whether the Raman contribution is included. Moreover, considerably energy is shed in the form of dispersive waves during this energy transfer.

Polarization of the solitons is also found to be affected considerably by the fiber's birefringence. Even if the two solitons are identically polarized initially, their SOP evolves along different trajectories on the Poincaré sphere as they interact nonlinearly. Polarization of both solitons is found to be affected considerably by the fiber nonlinearity in the case of medium birefringence, but linear effects dominate its evolution in fibers with large birefringence. We also varied the initial SOP of the two solitons by changing the angles θ and ψ in Eq. (15) and (16), the qualitative behavior seen in Figs. (1) to (9) remains nearly the same is all cases.

Finally we varied the relative phase of two input solitons because the soliton interaction is known to be phase sensitive. We found that the leading soliton always loses energy and transfers some of it to the trailing soliton. A good fraction of both soliton's energy is also shed in the form of dispersive waves. The situation becomes worse as the magnitude of birefringence increases. In some specific cases, a vector soliton lose as much as 70% of its energy to dispersive waves.

It should be stressed that we used a specific form of two input solitons given in Eqs. (15) and (16). As seen in the top row of Fig. 1, no radiation is emitted for such vector solitons in the absence of the TOD, Raman, and birefringence effects. When these effects are present, two vector solitons shed radiation in the form of dispersive waves. It may be possible to reduce this radiation by changing the form of the two input pulses.

[1] J. P. Gordon, "Interaction forces among solitons in optical fibers," Opt. Lett. **8**, pp. 596-598 (1983).

[2] F. M. Mitschke and L. F. Mollenauer, "Experimental observation of interaction forces between solitons in optical fibers," Opt. Lett. **12**, pp. 355-357 (1987).

[3] Y. Kodama and K. Nozaki, "Soliton interaction in optical fibers," Opt. Lett. **12**, pp. 1038-1040 (1987).

[4] T. Georges and F. Favre, "Modulation, filtering , and initial phase control of interacting solitons," J. Opt. Soc. Am. B **10**, pp. 1880-1889 (1993).

[5] G. P. Agrawal, *Nonlinear Fiber Optics*, 5th ed. (Academic Press, 2013).

[6] S. Kumar, A. Selvarajan and G. V. Anand, "Influence of Raman scattering on the cross phase modulation in optical fibers," Opt. Commun. **102**, pp. 329-335 (1993).

[7] A. Hause and F. Mitschke, "Reduced soliton interaction by Raman self-frequency shift," Phys. Rev. A **80**, 063824 (2009).

[8] M. F. Saleh, A. Armaroli, A. Marini and F. Biancalana, "Strong Raman-induced noninstantaneous soliton interactions in gas-filled photonic crystal fibers," Opt. Lett. **40**, pp. 4058-4061 (2015).

[9] P. Balla, S. Buch, and G. P. Agrawal, "Effect of Raman scattering on soliton interactions in optical fibers," J. Opt. Soc. Am. B **34**, 1247-1254 (2017).

[10] C. R. Menyuk, "Stability of solitons in birefringent optical fibers. I: Equal propagation amplitudes," Opt. Lett. **12**, 614-616 (1987).

[11] C. R. Menyuk, "Stability of solitons in birefringent optical fibers. II. Arbitrary amplitudes," J. Opt. Soc. Am. B **5**, 392-402 (1988).

[12] M. N. Islam, C. D. Poole, and J. P. Gordon, "Soliton trapping in birefringent optical fibers," Opt. Lett. **14**, 1011-1013 (1989).

[13] E. Korolev, V. N. Nazarov, D. A. Nolan, and C. M. Truesdale, "Experimental observation of orthogonally polarized time-delayed optical soliton trapping in birefringent fibers," Opt. Lett. **30**, 132-134 (2005).

[14] D. N. Christodoulides and R. I. Joseph, "Vector solitons in birefringent nonlinear dispersive media," Opt. Lett. **13**, 53-55 (1988).

[15] M. V. Tratnik and J. E. Sipe, "Bound solitary waves in a birefringent optical fiber," Phys. Rev. A **38**, 2011-2017 (1988).

[16] Y. S. Kivshar, "Soliton stability in birefringent optical fibers: analytical approach," J. Opt. Soc. Am. B **7**, 2204-2209 (1990).

[17] M. Haelterman and A. P. Sheppard, "The elliptically polarized fundamental vector soliton of isotropic Kerr media," Phys. Lett. A **194**, 191-196 (1994).

[18] Y. Silberberg and Y. Barad, "Rotating vector solitary waves in isotropic fibers," Opt. Lett. **20**, 246-248 (1995).

[19] J. M. Soto-Crespo, N. N. Akhmediev, and A. Ankiewicz, "Stationary solitonlike pulses in birefringent optical fibers," Phys. Rev. E **51**, 3547-3555 (1995).

[20] Yijiang Chen and Javid Atai, "Femtosecond soliton pulses in birefringent optical fibers," J. Opt. Soc. Am. B **14**, 2365-2372 (1997).

[21] Y. Bard and Y. Silberberg, "Polarization evolution and polarization instability of solitons in birefringent optical fibers," Phys. Rev. Lett. **78**, 3290-3293 (1997).

[22] B. A. Malomed and S. Wabnitz, "Soliton annihilation and fusion from resonant inelastic collisions in birefringent optical fibers," Opt. Lett. **16**, 1388-1390 (1991).

[23] B. A. Malomed, "Inelastic collisions of polarized solitons in a birefringent optical fiber," J. Opt. Soc. Am. B **9**, 2075-2082 (1992).

[24] X. D. Cao and D. D. Meyerhofer, "Soliton collisions in optical birefringent fibers," J. Opt. Soc. Am. B **11**, 380-385 (1994).

[25] C. De Angelis and S.Wabnitz, "Interactions of orthogonally polarized solitons in optical fibers," Opt. Commun. **125**, 186-196 (1996).

[26] Y. Tan and J. Yang, "Complexity and regularity of vector-soliton collisions," Phys. Rev. E **64**, 056616 (2001).

[27] R, Goodman and R. Haberman, "Vector-soliton collision dynamics in nonlinear optical fibers," Phys. Rev. E **71** 056605 (2005).

[28] J. Scheuer and M. Orenstein, "Forces and equilibrium states between interacting vector solitons," J. Opt. Soc. Am. B **18**, 954-959 (2001).

[29] M. Delqu'e, G. Fanjoux, and T. Sylvestre, "Collision between scalar and vector spatial solitons in Kerr media," Opt. Quant. Electron. **40** 281-291 (2008).

[30] S. T. Cundiff, B. C. Collings, and W. H. Knox, "Polarization locking in an isotropic, modelocked soliton Er/Yb fiber laser," Opt. Express **1**, 12-20 (1997).

[31] B. C. Collings, S. T. Cundiff, N. N. Akhmediev, J. M. Soto-Crespo, K. Bergman, and W. H. Knox, "Polarization-locked temporal vector solitons in a fiber laser: experiment," J. Opt. Soc. Am. B **17**, 354-365 (2000).

[32] L. M. Zhao, D. Y. Tang, H. Zhang, X. Wu, and N. Xiang, "Soliton trapping in fiber lasers," Opt. Express **16**, 9528-9533 (2008).

[33] S. V. Sergeyev, C. Mou, A. Rozhin, and S. K. Turitsyn, "Vector solitons with locked and precessing states of polarization," Opt. Express **20**, 27434-27440 (2012).

[34] C. Mou, S. V. Sergeyev, A. G. Rozhin, and S. K. Turitsyn, "Bound state vector solitons with locked and precessing states of polarization," Opt. Express **21**, 26868-26875 (2013).

[35] V. Tsatourian, S. V. Sergeyev, C. Mou, A. Rozhin, V. Mikhailov, B. Rabin, P. S. Westbrook, and S. K. Turitsyn, "Polarisation dynamics of vector soliton molecules in mode locked fiber laser," Sci. Rep. **3**, 3154 (2013).

[36] L. M. Zhao, D. Y. Tang, H. Zhang, and X. Wu, "Bound states of vector dissipative solitons," IEEE Photon. J **7**, 7802208 (2015).

[37] Y. Luo, J. Cheng, B. Liu, Q. Sun, L. Li, S. Fu, D.n Tang, L. Zhao, and D. Liu, "Group-velocity-locked vector soliton molecules in fiber lasers," Sci. Rep. **7** 2369 (2017).

[38] E. R. Martins, D. H. Spadoti, M. A. Romero, and B.-H. V. Borges, "Theoretical analysis of supercontinuum generation in a highly birefringent D-shaped microstructured optical fiber," Opt. Express **15**, 14335–14347 (2007).

[39] R. C. Herrera and C. T. law, "Dispersive waves in birefringent nonlinear fiber optics," Opt. Eng. **52**, 015007 (2013).

[40] Q. Lin and G. P. Agrawal, "Raman response function for silica fibers," Opt. Lett. **31**, 3086 (2006).

[41] J. Hult, J. Lightwave Technol. **25**, 3770 (2007).

[42] W. Yang, J. P. Snyder, and W. Tobler, "Map Projection Transformation: Principles and Applications," (CRC Press, 1999).